**Atmospheric
Chemistry
and Physics**
Discussions

Open Access

Stratospheric ozone trends and variability as seen by SCIAMACHY during the last decade

C. Gebhardt[1], A. Rozanov[1], R. Hommel[1], M. Weber[1], H. Bovensmann[1], J. P. Burrows[1], D. Degenstein[2], L. Froidevaux[3], and A. M. Thompson[4]

[1]Institute of Environmental Physics (IUP), University of Bremen, Bremen, Germany
[2]University of Saskatchewan, Saskatoon, Canada
[3]Jet Propulsion Laboratory, California Institute of Technology, Pasadena, USA
[4]Department of Meteorology, Pennsylvania State University, Pennsylvania, USA

Correspondence to: C. Gebhardt (gebhardt@iup.physik.uni-bremen.de)

Discussion Paper | Discussion Paper | Discussion Paper | Discussion Paper

ACPD

13, 11269–11313, 2013

Stratospheric ozone trends and variability

C. Gebhardt et al.

Title Page

Abstract	Introduction
Conclusions	References
Tables	Figures

◄◄   ►►

◄   ►

Back   Close

Full Screen / Esc

Printer-friendly Version

Interactive Discussion

Abstract

Vertical profiles of the rate of linear change (trend) in the altitude range 15–50 km are determined from decadal O_3 time series obtained from SCIAMACHY/ENVISAT measurements in limb viewing geometry. The trends are calculated by using a multivariate
5   linear regression in the zonal bands $5°$ S–$5°$ N (tropics), 50-60° N, and 50–60° S (mid- to high latitudes). Seasonal terms, the quasi-biennial oscillation, and solar cycle variations are accounted for in the regression. In the tropics, positive trends between 15 and 30 km and negative trends between 30 and 35 km are identified. Moderately positive O_3 trends are found in the upper stratosphere of the tropics and midlatitudes.
10 The explanation favoured for the observed positive and negative trends in the tropical lower and middle stratosphere is NO_x chemistry. Comparisons between SCIAMACHY and EOS MLS in the tropics and at midlatitudes show good agreement. In the tropics, measurements from OSIRIS/Odin and SHADOZ are analysed resulting in very similar vertical profiles of the rate of linear change of O_3. Observed trends in the stratospheric
15 column derived from integrated SCIAMACHY limb O_3 profiles and nadir total columns are found to be consistent.

1   Introduction

The Earth is shielded from UVB and UVC radiation in the 240–320 nm range by O_3 absorption in the stratosphere. This absorbed energy is the main heat source of the
20 stratosphere, which also drives the atmospheric circulation in the upper atmosphere (e.g. Weber et al., 2011). The abundance of O_3 is sensitive to various chemical and dynamical factors. The most prominent example for human impacts on the O_3 layer is the Antarctic O_3 hole caused by anthropogenically released chlorine and bromine compounds. In order to diminish the anthropogenic O_3 depletion, halogenated source
25 gases have been banned by the Montreal Protocol of 1987 and its amendments. A slowdown of the O_3 decline and even the onset of a recovery have been deduced

from observations (Reinsel, 2002; Newchurch et al., 2003; Yang et al., 2006; WMO, 2007). The recovery of the global stratospheric O_3 layer to values observed before the CFC-driven O_3 depletion is, however, not expected before the middle of this century (WMO, 2011).

Measurements of O_3 have a long tradition and various trend studies have been performed over the last few decades (WMO, 2007, and references therein). In recent years, several trend studies have aimed at investigating the impacts of O_3 depleting substances (ODS) and dynamical forcings affecting the O_3 shield (e.g. Reinsel et al., 2005; Rosenfield et al., 2005; Andersen et al., 2006; Miller et al., 2006; Steinbrecht et al., 2006; Dhomse et al., 2006; Zanis et al., 2006; Randel and Wu, 2007; Harris et al., 2008; Jones et al., 2009; WMO, 2007, 2011). The majority of these trend assessments agreed that the present stage of O_3 is somewhere between its depletion slowing down and the subsequent turnaround phase, expected as a result of the measures implemented within the Montreal Protocol and its amendments. The complexity of the issue of the longterm evolution of stratospheric O_3 arises from stratospheric O_3 being influenced by several factors which vary with latitude and altitude. For gas phase catalytic O_3 depletion, major groups of catalytic species were identified with the partitioning of the species varying with altitude. These are HO_x (Bates and Nicolet, 1950), NO_x (Crutzen, 1970), ClO_x (Stolarski and Cicerone, 1974; Molina and Rowland, 1974), and BrO_x (McElroy et al., 1986). The altitude dependence of their partitioning in O_3 depletion is discussed in Osterman et al. (1997).

The observation of high latitude loss of O_3 in springtime (Farman et al., 1985) has been the source of much study and led to our current scientific understanding of O_3 (WMO, 2011, and references therein). This manuscript contributes to our knowledge of stratospheric O_3 and its changes during the period following the turnaround in stratospheric halogens in the late 1990s where the halogen load, still high, is slowly declining.

Vertically resolved O_3 trends are derived from observations by satellite instruments, groundbased lidars and microwave radiometers, and balloon-borne ozonesondes (Steinbrecht et al., 2006; Jones et al., 2009; Randel and Thompson, 2011; Mieruch

et al., 2012). In Mieruch et al. (2012), O_3 trends from SCIAMACHY and those inferred from a range of instruments were compared within the period from 2002 to 2008. Therein, it was shown that trend comparison results are not significantly changed when comparing collocated measurement pairs and gridded monthly mean values. It was demonstrated further that inter-instrumental trend comparisons are needed to assess instrumental issues like detector degradation or line of sight mispointing. A number of satellite datasets of O_3 were investigated by Jones et al. (2009). There, O_3 trends were inferred from an average dataset including various satellite instruments between 1979 and 2008. SCIAMACHY, OSIRIS/Odin, and EOS MLS contributed to the years after 2000. Jones et al. (2009) showed that these satellite data agreed with each other to a high extent. After 1997, Jones et al. (2009) identified moderately positive midlatitude O_3 trends between 35 and 45 km in the order of a few percent per decade. These findings are corroborated by Steinbrecht et al. (2006, 2009) by using groundbased measurements. As the upper stratosphere is highly sensitive to halogen chemistry (WMO, 1999), these may be signs for the onset of a turnaround in the O_3 abundance in response to declining halogens. Analysing a merged dataset from satellites and ozonesondes, Randel and Thompson (2011) identified some negative O_3 trends in the lowermost tropical stratosphere. These were attributed to dynamical factors, namely enhanced tropical upwelling.

In this study, a global O_3 dataset obtained from the SCIAMACHY instrument on board ENVISAT is investigated. SCIAMACHY was in routine operation from August 2002 until ENVISAT suddenly and unexpectedly failed on 8 April 2012. In its limb viewing geometry, SCIAMACHY performed measurements of the scattered solar radiation. Limb measurements are used to retrieve vertical profiles of atmospheric constituents, i.e. trace gases, aerosols, and clouds (Sioris et al., 2003, 2004; Rozanov et al., 2007, 2011; Kühl et al., 2008; Bauer et al., 2012; Ernst et al., 2012). Besides SCIAMACHY, the profiling instruments ACE FTS (Bernath et al., 2005), ACE MAESTRO (Bernath et al., 2005), EOS MLS (Jarnot et al., 2006), GOMOS (Kyrölä et al., 2004), HALOE (Russell et al., 1993), HIRDLS (Gille et al., 2003), MIPAS (Fischer et al., 2008), OSIRIS/Odin

(Llewellyn et al., 2004), POAM III (Lucke et al., 1999), SAGE II (Mauldin et al., 1985), SMILES (Kikuchi et al., 2010), and SMR (Murtagh et al., 2002) made measurements during the last decade.

Rates of linear change or trends in the SCIAMACHY limb O_3 time series are inferred in our investigation for the period from August 2002 to December 2011. The trends are presented as functions of altitude and latitude. The trends from SCIAMACHY are compared with those derived from OSIRIS/Odin, EOS MLS, and SHADOZ ozonesondes. The instrument comparisons are based on monthly mean time series without any temporal collocation criteria between the instruments. The resulting O_3 trend profiles are presented for selected latitude bands in the tropics and at midlatitudes. In addition, trends in the integrated O_3 column from SCIAMACHY limb and merged total O_3 from GOME (Burrows et al., 1999), SCIAMACHY nadir, and GOME2 (Callies et al., 2000) are compared.

This manuscript is structured as follows. Section 2 provides an overview about the SCIAMACHY limb O_3 retrieval. The multivariate linear regression, used in our study, is introduced and explained in Sect. 3. The O_3 time series from SCIAMACHY and their regression models are described in Sect. 4. In Sect. 5, the vertical profiles of the rate of linear change or trend of the O_3 retrieved from SCIAMACHY measurements are presented. O_3 trend profiles from SCIAMACHY are compared with those from EOS MLS and OSIRIS/Odin, other atmospheric limb sounders, in Sect. 6. In Sect. 7, further comparisons are performed in the tropics including SHADOZ ozonesondes and column integrated O_3. Section 8 summarizes the main results of the study.

2 SCIAMACHY limb ozone

The European environmental research satellite ENVISAT hosted ten instruments, which were operational until its abrupt loss on 8 April 2012. SCIAMACHY recorded electromagnetic radiation upwelling from the Earth's atmosphere in 3 measurement modes: occultation, nadir, and limb geometry. Detailed information is provided in

Burrows et al. (1995) and Bovensmann et al. (1999). In limb viewing geometry, the instrument scanned the horizon in 3.3 km steps. Each limb scan sequence ranged from −3 to 92 km (0 to 92 km since October 2010) in tangent height. The vertical sampling and the instantaneous field of view (2.6 km × 103 km) defined the vertical resolution of typically 3–4 km. Global coverage was achieved within 6 days at the equator and less elsewhere. ENVISAT was in a sun-synchronous orbit with an inclination of 98° and it overpassed geolocations between 82° N and 82° S during daytime (less in the winter hemisphere).

Our investigation uses a monthly mean dataset of O_3 which was binned into zonal means of the following latitude bands: 60–50° N, 5° N–5° S, and 50–60° S. The boundaries of 60° N and 60° S are chosen for this investigation to avoid any effects which are directly related to the polar vortex. Some of the inter-instrumental comparisons presented in the manuscript also cover the 20° N–20° S latitude band. In order to avoid possible influences of the South Atlantic Anomaly, any data within the longitudes of 285° and 345° and latitudes of 20° S and 60° S are excluded. For each latitude band, the rate of linear change or trend of O_3 has been determined for all altitudes between 15 and 50 km resulting in a O_3 trend profile.

The SCIAMACHY results presented here use the limb O_3 retrieval version 2.5 of IUP Bremen. O_3 is retrieved in 1 km steps from 10 to 75 km. The derived rate of linear change or trend profiles are presented in steps of 1 km accordingly. With the satellite retrieval often suffering from cloud interference below 15 km, only altitudes above 15 km are taken into consideration in the following.

3 Trend determination

3.1 Multivariate linear regression

A multivariate linear regression is applied to the datasets with autocorrelations of consecutive values accounted for by the Cochrane–Orcutt transformation (Cochrane and

Stratospheric ozone trends and variability

C. Gebhardt et al.

Title Page

Abstract | Introduction

Conclusions | References

Tables | Figures

◀ | ▶

◀ | ▶

Back | Close

Full Screen / Esc

Printer-friendly Version

Interactive Discussion

Orcutt, 1949). The regression is unweighted. The following terms are used in the regression:

$$\mu + \omega t + \sum_{j=1}^{4}\left(\beta_{1j}\sin\left(\frac{2\pi jt}{12}\right) + \beta_{2j}\cos\left(\frac{2\pi jt}{12}\right)\right) + \Delta(t), \tag{1}$$

where t is the time in months and μ, ω, and $\beta_{11}, \beta_{12}, \ldots, \beta_{24}, \beta_{24}$ are fitting parameters. The harmonics with 12, 6, 4, and 3 month periods, $j = 1, 2, 3, 4$, a sine and cosine term each, are used to represent seasonal changes. Clearly, harmonics of 12 and 6 months approximate the annual and semi-annual cycles. The combination of sine and cosine terms provides a flexible adjustment to any phase of the (semi-)annual variation. As discussed by Stiller et al. (2012), as the oscillation patterns are possibly compressed or stretched with respect to a harmonic shape, the terms having 4 and 3 month periods improve the fit quality. In addition, a linear fit having a gradient or slope ω and an intercept μ is included in the regression analysis. The gradient is the O_3 trend at a given altitude. Its standard deviation is the 1σ value of the error, which is also used for the error bars of trends in subsequent figures. It comprises fluctuations due to instrumental errors as well as natural variability. The trends are given in units of $\%\,yr^{-1}$ with respect to the mean value of the time series. The criterion for the trend being significant to the 95 % confidence level is that the absolute ratio of the trend to its standard deviation is larger than 2 (Tiao et al., 1990). As discussed in Sect. 3.2, it is also advantageous to extend the linear regression, see Eq. (1), by additional terms representing the quasi-biennial oscillation (QBO) and the solar cycle (SC):

$$\Delta(t) = QBO(t) + SC(t). \tag{2}$$

In the northern midlatitudes, there is an exception from Eq. (1) because of the strong interannual variability of the annual cycle of O_3. In the 15–26 km range of the 60–50° N zonal band, the cumulative eddy heat flux (based on ERA-Interim, 50 hPa eddy heat flux integrated from 45° N to 75° N, cumulation starts in October) is fitted instead of harmonic terms. The cumulative eddy heat flux is a proxy accounting for the wave driven

11275

O_3 accumulation in winter and early spring. For 60–50° N, the interannual variability in total O_3 is found to be well approximated by the cumulative eddy heat flux (Dhomse et al., 2006). Here, correlation tests show that throughout the altitude range from 15–26 km, a time lag of 2 months is optimum.

3.2 The QBO signal of ozone

The quasi-biennial oscillation (QBO) is a quasi-periodic signal observed in the tropical stratospheric zonal wind speed. It alternates between east and west phase with the period varying between 2 and 3 yr. Previous studies report a maximum QBO response of tropical O_3 in the altitude ranges of 20–27 km and 30–38 km (Zawodny and McCormick, 1991; Chipperfield et al., 1994).

In the tropics, the QBO response of O_3 is driven by effects related to the vertical transport (Butchart et al., 2003). As described by the thermal wind relation, a QBO signal is induced in the temperature and meridional circulation. The QBO induced meridional circulation modulates the upwelling branch of the Brewer–Dobson circulation. This modulation of the tropical upwelling leads to the largest changes of the O_3 volume mixing ratio (VMR) in the altitude range of large vertical gradients of the O_3 VMR, which are located below and above the maximum in the vertical O_3 VMR profiles. The result is a compacting (vertical squeezing) of the mean vertical O_3 VMR profile at westerly QBO phase and a lofting (vertical stretching) at easterly phase. Around the maximum of the mean vertical profile of the O_3 VMR, where the vertical gradient changes sign, the phase change of the QBO response of O_3 takes place (Butchart et al., 2003). With the QBO phases modulating the Brewer–Dobson circulation, a QBO response may be observed in extratropical O_3 as well (Baldwin et al., 2001).

The Singapore winds are extensively used as a QBO proxy to describe the temporal evolution of stratospheric O_3 and assess accompanied trends. The radiosonde measured Singapore wind time series (available from http://www.geo.fu-berlin.de/en/met/ag/strat/produkte/qbo/) cover pressure levels up to 10 hPa (Naujokat, 1986). In the following, the 10 hPa and 30 hPa Singapore winds are used as fit proxies, i.e.:

Printer-friendly Version

Interactive Discussion

$$QBO(t) = a\,QBO_{10}(t) + b\,QBO_{30}(t), \qquad\qquad\qquad (3)$$

with a and b as their fit coefficients. The indices "10" and "30" denote the pressure level of the proxy. This approach is applied both in the tropics and extratropics to account for any QBO effects.

5   The monthly time series of the Singapore winds are smoothed by a 12 month running average before being used as QBO proxy. The same is done with the Mg II index, used as a solar cycle proxy. Both proxies are not detrended.

3.3   The solar cycle of ozone

The 11 yr solar cycle, which leads to pronounced variations of the solar radiation in the
10   UV spectral range, is known to be reflected by stratospheric O_3 (Gray et al., 2010). It is widely accepted that the solar cycle response of O_3 occurs without any time lag and at positive correlation (e.g. Soukharev and Hood, 2006; Remsberg and Lingenfelser, 2010). The solar cycle response of O_3 may extend from the tropics into the midlatitudes (SPARC CCMVal, 2010). In the following, a solar cycle proxy is included in the
15   multivariate linear regression for any latitude band analysed.

      Among the most popular proxies for the solar cycle response of O_3 are the Mg II index and F10.7 cm flux (Fioletov, 2009). As discussed by Viereck et al. (2001, 2004), the Mg II index shows excellent correlation with solar UV radiances. In the following, a multi-instrument monthly average MgII index is used, which is mainly based on
20   GOME, SCIAMACHY, and GOME2 observations over the time span under study. The data can be obtained from http://www.iup.uni-bremen.de/gome (Weber et al., 2013).

      In addition to the QBO and the solar cycle, the O_3 time series might also be influenced by the El Niño Southern Oscillation (ENSO) (Randel et al., 2009; Lee et al., 2010; Randel and Thompson, 2011; Thompson et al., 2011). However, for SCIA-
25   MACHY limb O_3, no clear signatures of ENSO were identified in the time series using either the MEI (http://www.esrl.noaa.gov/psd/enso/mei/table.html) or the OEI index (Ziemke et al., 2010) as proxy.

4   Time series of ozone

Figures 1 to 4 show O_3 time series at the altitudes of 35 km and 44 km at northern midlatitudes (60–50° N) and in the tropics (5° N–5° S). The time series are overlaid by their fitting curve from our regression model: the fit residuals being plotted below. The individual terms from the regression, i.e. the harmonics, QBO, and solar cycle related contributions, are shown in separate panels. The harmonic terms are overlaid by the time series with the linear fitting terms subtracted (i.e. a detrended time series) and the QBO terms by the time series with the linear and harmonic fitting terms subtracted (i.e. a detrended and deseasonalised time series). For the solar cycle terms, all terms but the solar cycle are removed from the overlaid time series.

At both altitudes, good fit quality is obtained. The use of harmonics for approximating the (semi-)annual oscillation as well as the combination of the 10 hPa and 30 hPa Singapore winds to proxy QBO appears to be a sufficiently complete approach. The fit residuals are well within ±5 % to ±10 % of the fitted time series both at midlatitudes and in the tropics.

At 35 km at midlatitudes, the annual cycle terms dominate in the fitting curve. The O_3 maximum is reached in late spring/early summer persisting for the summer months. At 44 km at midlatitudes, the harmonic terms have two maxima and minima per year. The annual minimum occurs in summer and a secondary minimum in winter. These patterns are explained as follows: The periodic variability of O_3 is governed by photochemical O_3 production at 35 km and catalytic O_3 depletion at 44 km, both being on its maximum in summer (Perliski et al., 1989). At 35 km, the annual maximum in summer driven by photochemical production is flattened by catalytic depletion which is of minor consequence. At 44 km, catalytic depletion has gained control leading to the annual minimum in summer. Overlaid photochemical production leads to a secondary minimum in winter.

At 35 km in the tropics, the QBO and semi-annual terms dominate. As discussed before, the maximum QBO response of tropical O_3 is located below 40 km. With

Title Page

Abstract | Introduction

Conclusions | References

Tables | Figures

|◄ | ►|

◄ | ►

Back | Close

Full Screen / Esc

Printer-friendly Version

Interactive Discussion

increasing altitude, the semi-annual oscillation predominates. At 44 km in the tropics, the semi-annual terms provide the most important contribution to the fitting curve. In the middle tropical stratosphere, the semi-annual oscillation of O_3 is driven by photochemical O_3 production which reflects two equator passages of the sun per year (Perliski et al., 1989). In the upper tropical stratosphere, a semi-annual oscillation is also observed in the zonal winds and temperatures, known as the stratospheric semi-annual oscillation (SAO).

5 Resulting trends and discussion

5.1 Tropical and extratropical trend profiles

The O_3 trend profiles and estimated errors (both in $\% \, yr^{-1}$) for the three latitude bands are shown in Fig. 5. Three features of particular interest are identified:

– a distinct positive trend in the tropics between 15 and 30 km

– a distinct negative trend in the tropics between 30 and 35 km

– a moderately positive trend in the upper tropical stratosphere between 38 and 48 km and at northern midlatitudes (between 40 and 45 km).

In the lower tropical stratosphere, the observed positive trends have their maximum of $1 \, \% \, yr^{-1}$ around 20 km. This maximum is fairly broad in altitude. From 20 to 28 km, the 95 % significance criterion is met. In the middle tropical stratosphere, the negative trends reach a maximum of $-2 \, \% \, yr^{-1}$ around 33 km. In the upper tropical stratosphere, moderately positive trends of around $0.5 \, \% \, yr^{-1}$ are observed.

At northern and southern midlatitudes, the trends do not exceed $\pm 1 \, \% \, yr^{-1}$ in the altitude range from 20 to 50 km. The northern trend profile is more variable with several sign changes of the trend. Moderately positive trends of around $0.5 \, \% \, yr^{-1}$ are seen between 40 and 45 km. The southern trends are close to zero for almost all altitudes.

The trend errors are comparable for all three latitude bands. There is some asymmetry between 60–50° N and 50–60° S. The northern trends reach almost $-1\,\%\,yr^{-1}$ in the 25–35 km range while the southern trends are close to zero in the same altitude range.

In the tropics, the QBO and solar cycle proxies are included sequentially into the regression model in order to investigate their influence on the resulting trend profile. The QBO is followed by the solar cycle, as shown in Fig. 6. Including the QBO, the trend errors are clearly reduced at all altitudes below 40 km. Between 20 and 30 km, the trends increase notably by up to $0.5\,\%\,yr^{-1}$. With the solar cycle considered, notable changes to the tropical trend profile occur above 35 km. The trends become different from zero and reach values of around $0.5\,\%\,yr^{-1}$ between 38 and 48 km.

5.2 Factors relevant to explaining the O_3 trends

In the tropical stratosphere between 15 and 30 km, both dynamical and chemical factors potentially explain the positive O_3 trends observed by SCIAMACHY. For example, changes in the rate of tropical upwelling, changes in halogens, or changes in NO_x are possibly responsible for changes in O_3. Analysing O_3 partial columns between 18 and 25 km, Yang et al. (2006) found that halogens are of minor importance in this altitude range because many CFCs do not release their radicals immediately after their injection through the tropical tropopause. Since the vertical gradient of O_3 is positive, enhanced vertical advection has a negative O_3 response in the lower tropical stratosphere. Randel and Thompson (2011) suggested that an increase of the tropical upwelling has led to some negative O_3 trends around 17 km to 21 km observed in the period 1984–2009. As the O_3 trends seen by SCIAMACHY are positive and spread over a much wider altitude range, an increase in vertical advection related to the tropical upwelling may be masking in part the increase in O_3, which must have another explanation. According to Nevison et al. (1999), an increase in NO_x might be a reason for a positive trend in O_3 at these altitudes. This is because NO_x trigger buffering effects as a result of interactions with HO_x and ClO_x cycles beside catalytic O_3 depletion. Nevison et al. (1999) have shown that an increase in NO_x results in an O_3 enhancement

extending up to around 30 km in the proximity of the equator and holding well below 20 km. This altitude range coincides with the positive O_3 trends observed by SCIA-MACHY.

In the 30–35 km range, NO_x can also be a potential driver for negative trends observed in tropical O_3 by SCIAMACHY. In particular, Portmann and Solomon (2007) and Fleming et al. (2011) have performed model sensitivity studies with increasing the N_2O source of NO_x. Both studies predicted the most negative O_3 response near 35 km in the tropics. The latitudinal extent of the modelled maximum O_3 response depends on the model scenario assumed. Different model scenarios imply different NO_x emissions for the future. For example, the model run of Fleming et al. (2011) for the time span 1979–1996 results in a broad maximum response between 50° N–50° S while a narrow maximum response centred around the equator is seen for the period 2005–2095 (their Figs. 3 and 4). The negative O_3 trends observed by SCIAMACHY for 2002–2011 decay to approximately half of their value from 5° N–5° S to 20° N–20° S as shown in Sect. 6.3.

Figure 7 shows a latitude-altitude cross section of the O_3 trends spanning the latitude range from 70° N to 70° S. The cross section is based on zonally averaged O_3 data binned in 5° latitude bins. As a function of the latitude, the trends are shown for the 15 to 50 km altitude range. As before, there are distinct positive trends between 15 and 30 km and distinct negative trends between 30 and 35 km in the tropics. Moderately positive trends in the upper stratosphere, identified before for 5° N–5° S between 38 and 48 km and also for 60–50° N between 40 and 45 km, are observed over large parts of the latitude range from 70° N to 70° S. The hemispheric asymmetry at midlatitudes between 25 and 35 km is clearly pronounced with negative trends in the Northern Hemisphere and positive trends in the Southern Hemisphere. Below 20 km, some positive trends not considered before are evidenced (around 70-60° N, 30° S, 60–70° S). These trends should, however, be treated with caution because of potential impact of clouds possibly reaching up to 20 km (Mieruch et al., 2012).

Moderately positive O_3 trends of approximately 0.5 % yr^{-1} are inferred from SCIA-MACHY in the upper stratosphere over large parts of the tropics and midlatitudes. As

Stratospheric ozone trends and variability

C. Gebhardt et al.

Title Page

Abstract	Introduction
Conclusions	References
Tables	Figures

|◀ | ▶|

| ◀ | ▶ |

| Back | Close |

Full Screen / Esc

Printer-friendly Version

Interactive Discussion

O$_3$ in the upper stratosphere is highly sensitive to halogens (WMO, 1999), these trends are expected to be in response to declining halogens. Evidence for a turnaround in upper stratospheric O$_3$ has already been pointed out by Reinsel (2002). Some attribution to declining halogens has been provided by Newchurch et al. (2003). Their study is based on satellite data indicating at least a levelling off of O$_3$ for the tropics and in the extratropics. Meanwhile the O$_3$ abundance continuing some levelling off or slight increase has been supported by various groundbased lidar and microwave radiometer stations (Steinbrecht et al., 2006, 2009).

A potential explanation for the asymmetry between the northern and southern trend profiles, negative trends and positive trends between 25 and 35 km, respectively, is provided by age of air results from Stiller et al. (2012) based on MIPAS data covering the same observation period as SCIAMACHY. In the northern non-polar middle stratosphere, a clear increase of the mean age of air has been observed. This may be explained by in-mixing of polar vortex air after sudden stratospheric warmings. This implies some dilution of O$_3$ in the altitude range in question.

6 Comparisons of trends from SCIAMACHY with those from other limb measurements

6.1 OSIRIS/Odin

The Odin satellite, which carries the OSIRIS instrument (Llewellyn et al., 2004), follows a near terminator orbit so that the illumination conditions specific to OSIRIS are always close to the solar terminator. The ascending node was constantly between 6 and 7 p.m. over the time span considered here. Similar to SCIAMACHY, OSIRIS measures the scattered solar light in limb viewing geometry. Seasonal variations of day and night times interrupt the OSIRIS measurements in the winter hemisphere. As a result, OSIRIS provides continuous time series only in the tropics. The data might also be unequally distributed around the equator, i.e. predominantly to the north from

it during northern summer and vice versa. Thus, the upcoming comparison between the instruments is performed with the tropics represented by the 20° N–20° S band. In order to match the sampling of both instruments, their data are first binned horizontally in 5° latitude × 15° longitude. The data from both instruments are excluded in any bin if one of the instruments has no data for the corresponding month and altitude. Subsequently, the zonal monthly means for the 20° N–20° S band are calculated. The time span covered by the comparison is August 2002–December 2011.

The OSIRIS O_3 data are from the retrieval version 5.07 produced by the University of Saskatchewan, which has a modified filtering of outliers with respect to earlier versions. The OSIRIS data separate clearly into records at AM and PM local time. As pointed out by Huang et al. (2010), diurnal variations of O_3 are expected to be in the order of only a few percent in the stratosphere. Because the equator crossing time of Odin is closer to that of ENVISAT, the AM O_3 data from OSIRIS are used, which in any case are made closer in time to SCIAMACHY.

The retrieval altitudes of OSIRIS, which has a smaller vertical step and higher spatial resolution, and SCIAMACHY are between one another. For each altitude of SCIAMACHY from 15 to 50 km, the two adjacent altitudes of OSIRIS were interpolated to the SCIAMACHY altitude.

6.2 EOS MLS

The MLS instrument aboard the EOS Aura satellite (Jarnot et al., 2006) measures the radiation emitted by the Earth's atmosphere in the microwave spectral range on both the day and night side of the near-polar orbit. In this comparison, we have used O_3 profiles retrieved from MLS daytime measurements. Aura crosses the equator in ascending node at 1.45 p.m. local time. Its daytime measurements extend deep into both hemispheres similar to the measurements from SCIAMACHY. The comparison between the instruments is done for the latitude bands defined in Sect. 2, namely 60–50° N, 5° N–5° S, and 50–60° S. The time span for the comparison is August 2004–December 2011.

The MLS O_3 data used here are from the retrieval version 2.2. The pressure serves as the vertical coordinate. After conversion from pressure to geometric height, the MLS O_3 profiles are interpolated to the altitudes of the SCIAMACHY retrieval. Zonal monthly means are calculated for the 3 latitude bands between 15 and 50 km.

6.3 Trend comparisons

Figures 8 and 9 show the comparisons between SCIAMACHY and MLS at midlatitudes. At northern midlatitudes, the MLS O_3 trend profile has less variability with altitude than that of SCIAMACHY. There are some significant deviations between 30 and 35 km with SCIAMACHY showing a clear negative trend while MLS shows nearly zero positive trends. Moderately positive trends seen by SCIAMACHY around 40 to 45 km agree with MLS within the uncertainties. There is also reasonable agreement in the southern midlatitudes. The trend profiles from both instruments follow each other closely and have similar error bars. The agreement between SCIAMACHY and MLS holds up to 50 km, where both profiles become increasingly negative.

The comparison for the tropics, represented by the 5° N–5° S latitude band, is shown in Fig. 10. Both SCIAMACHY and MLS show negative trends in the tropical 30–35 km range with SCIAMACHY reaching $-2\,\%\,\mathrm{yr}^{-1}$ and MLS showing a maximum between $-1\,\%\,\mathrm{yr}^{-1}$ and $-1.5\,\%\,\mathrm{yr}^{-1}$. From 29 km down to 21 km, MLS confirms the positive trends seen by SCIAMACHY. However, the agreement is poorer below 21 km. This might be a result of vertical oscillations in the tropical UTLS region known since the early phase of version 2.2 MLS validations (Froidevaux et al., 2008). Some further discrepancies are observed in the 40–50 km range. Here, SCIAMACHY shows moderately positive trends of around $0.5\,\%\,\mathrm{yr}^{-1}$ while MLS points towards zero to slightly negative trends.

In Fig. 11, the comparison between SCIAMACHY and OSIRIS is shown. As described in Sect. 6.1, the wider tropical zonal band from 20° N to 20° S is investigated. The positive trends from OSIRIS between 15 and 30 km are in good agreement with those from SCIAMACHY. In the 30–35 km range, the negative trends seen

Discussion Paper | Discussion Paper | Discussion Paper | Discussion Paper

Title Page

Abstract | Introduction

Conclusions | References

Tables | Figures

|◄ | ►|

◄ | ►

Back | Close

Full Screen / Esc

Printer-friendly Version

Interactive Discussion

by SCIAMACHY for 20° N–20° S are somewhat weaker than those for 5° N–5° S: SCIA-MACHY reaches $-1\,\%\,yr^{-1}$ while the trends from OSIRIS are around $-0.3\,\%\,yr^{-1}$ at maximum. In the upper stratosphere, both SCIAMACHY and OSIRIS show moderately positive trends of around $0.5\,\%\,yr^{-1}$. This value is obtained for SCIAMACHY between 40 and 50 km and for OSIRIS near 40 km.

A three-instrument comparison between SCIAMACHY, OSIRIS, and MLS has also been performed. The latitude band of 20° N–20° S and the time span from August 2004 to December 2011 are selected for the comparison. The resulting trend profiles are shown in Fig. 12. In good agreement, SCIAMACHY, OSIRIS, and MLS show negative trends between 30 and 35 km. Below 30 km, the O_3 datasets from all three instruments have positive trends. Good agreement between the O_3 trends from SCIAMACHY, MLS, and OSIRIS is found down to around 20 km, where the O_3 trend from SCIAMACHY has its maximum. Below 20 km, the trends from SCIAMACHY decrease gradually towards zero whereas OSIRIS and MLS still increase.

7   Comparisons of trends from SCIAMACHY with those from independent measurement techniques

7.1   SHADOZ ozonesondes

As discussed above, the tropical trend profile from SCIAMACHY has the shape of a dipole: distinct positive trends being observed between 15 and 30 km and distinct negative ones between 30 and 35 km. A similar structure was observed in O_3 trends inferred from other satellite measurements. In this section, we compare the O_3 trends from SCIAMACHY with those from balloon-borne ozonesonde measurements.

The altitude range of the balloon sonde O_3 data is determined by the altitude at which the balloon bursts. Thus, few balloons achieve maximum altitudes above 30 km. The data from ozonesondes have a vertical resolution in the order of 100 m, clearly finer than that from the SCIAMACHY limb sounder, which is typically 3–4 km. The vertical O_3

Stratospheric ozone trends and variability

C. Gebhardt et al.

Title Page

Abstract | Introduction

Conclusions | References

Tables | Figures

|◄ | ►|

◄ | ►

Back | Close

Full Screen / Esc

Printer-friendly Version

Interactive Discussion

profiles from the sondes are smoothed over intervals of ±2 km relative to the altitudes defined by the O_3 retrieval from SCIAMACHY, i.e. from 15 to 30 km in steps of 1 km. In the following, these smoothed O_3 profiles are used for determining monthly averaged O_3 time series from the sondes.

5 SHADOZ is a network of more than 10 ozonesonde stations at (sub-)tropical sites (e.g. Thompson, 2003). Since coming into being in 1998, the network has been systematically operational with typically several ozonesonde launches per month per station. The datasets of all stations are freely accessible via http://croc.gsfc.nasa.gov/shadoz/. Here, we select the stations at Ascension (8.0° S, 14.4° W), Kuala Lumpur (2.7° N, 101.7° E), Nairobi (1.3° S, 36.8° E), Natal (5.4° S, 35.4° W), and Paramaribo (5.8° N, 55.2° W). According to their geolocations, these stations match the 5° N–5° S zonal band, considered before, quite well. The monthly averaged O_3 time series over all 5 stations are calculated. In order to account for possible offsets between the stations, the mean values of single-station time series are adjusted before averaging. The reference value is the mean value of one of the contributing stations, in our case Paramaribo. The resulting sonde trend profile is compared to the trend profile from SCIAMACHY, which is based on data selected at latitudes and longitudes around the sites of the ozonesonde stations and averaged accordingly.

Figure 13 compares the sonde and SCIAMACHY O_3 trend profile from 15 to 30 km.
20 As a result of the high zonal symmetry of tropical stratospheric O_3 (Thompson, 2003; Randel and Thompson, 2011), the trend profile from SCIAMACHY is very similar to the profile obtained for the entire 5° N–5° S zonal band in Sect. 5.1. There are positive trends between 15–30 km with a maximum around 20 km. By the sondes, positive trends are seen in the 15–30 km range as well. The O_3 trend uncertainties are comparable for both trend profiles at most altitudes. The sondes are in agreement with SCIAMACHY from 30 km down to around 20 km. Below 20 km, the trends from the sondes climb further and reach a maximum between 15–20 km. For SCIAMACHY, the O_3 trends decay continuously towards zero. The data from the sondes indicate a trend maximum somewhat lower than SCIAMACHY.

The differences between 15–20 km may arise from the satellite retrieval suffering from the impacts of high convective clouds, see e.g. Mieruch et al. (2012). Considering the last decade only, there is still some tendency towards positive O_3 trends in the lowermost tropical stratosphere in contrast to those trends inferred by Randel and Thompson (2011). Their O_3 trends were inferred from a dataset merged between SAGE II and SHADOZ spanning the period from 1984–2009. Some negative trends were identified in the lowermost tropical stratosphere and attributed to enhanced tropical upwelling.

7.2 Total ozone

A comparison of the trend in the stratospheric O_3 column derived by integrating SCIAMACHY limb O_3 with that in total column O_3 has been made for the period from August 2002 to December 2011. The total O_3 columns are obtained from a merged dataset from GOME, SCIAMACHY nadir, and GOME2 (Weber et al., 2012). The dataset is in good agreement with the O_3 observations from Dobson and Brewer data networks and also with the total O_3 data from SBUV and TOMS. This dataset of zonal mean total O_3 (GOME/SCIAMACHY/GOME2 merged WFDOAS total ozone V1) is accessible via http://www.iup.uni-bremen.de/gome/wfdoas. By averaging over 5° N–5° S, the monthly time series of tropical total O_3 is obtained and compared to the tropical SCIAMACHY limb O_3 integrated over the entire altitude range from 10 to 75 km.

With large parts of total O_3 residing in the stratosphere, the time series of integrated limb O_3 and total O_3 are quite close to each other as shown in Figs. 14 and 15. Due to tropospheric O_3 below 10 km, the GOME/SCIAMACHY/GOME2 total O_3 time series is always slightly larger than the integrated limb time series. Trend analyses including the QBO and solar cycle are performed for the integrated limb and merged total O_3, yielding trends of $(0.1 \pm 0.1)\,\%\,yr^{-1}$ and $(0.3 \pm 0.1)\,\%\,yr^{-1}$, respectively. Thus, a consistent near zero trend is observed for both integrated limb and nadir total O_3 in the inner tropics from 2002 to 2011. This results from the positive trend in the lower and upper stratosphere cancelled by the negative trend in the middle stratosphere. This unusual and

unexpected O_3 trend behaviour in the tropics as a function of altitude is not observable in the total column data.

8 Conclusions

Time series from vertical profiles of O_3 from SCIAMACHY limb measurements have been analysed for the 60–50° N, 5° N–5° S, and 50–60° S latitude bands. Rates of linear change or trends were determined for stratospheric O_3 in the 15–50 km range for the time span August 2002 to December 2011. The trends obtained from SCIAMACHY were compared to those obtained from the measurements of the OSIRIS/Odin and EOS MLS satellite instruments and to the trends from SHADOZ ozonesondes. SCIAMACHY and the comparison instruments are found to be in good agreement down to altitudes around 20 km.

In the tropics, the O_3 trend profile is found to exhibit a pronounced dipole shape. There are positive trends up to 1 % yr^{-1} between 15 and 30 km and negative trends up to -2 % yr^{-1} between 30 and 35 km. As identified by Nevison et al. (1999), positive O_3 trends observed between 15 and 30 km are likely to be caused by increasing NO_x. In agreement with the studies of Fleming et al. (2011) and Portmann and Solomon (2007), increasing NO_x are also favoured as driver of negative tropical O_3 trends observed between 30 and 35 km. Further studies on NO_2 trends from SCIAMACHY are underway to elucidate further the origin of the changes in the vertical profile of O_3 trends.

In the upper stratosphere between 40 and 50 km, moderately positive O_3 trends are seen by SCIAMACHY from the tropics to the midlatitudes of both hemispheres. These trends are believed to be in response to declining halogens as this region is highly sensitive to halogen chemistry (WMO, 1999). Similar O_3 trends have been previously reported by Steinbrecht et al. (2006, 2009), Jones et al. (2009), and WMO (2011) in the 35–45 km range.

In our study, integrated limb O_3 from SCIAMACHY has also been considered in order to assess the net effect of vertically resolved trends. Both SCIAMACHY integrated

limb O_3 and merged total O_3 from GOME, SCIAMACHY nadir, and GOME2 show consistently near zero trends in the tropics. For the considered time span, this is the net effect of positive O_3 trends in the lower and upper stratosphere and negative O_3 trends in the middle stratosphere seen in the vertically resolved time series. This finding is also compliant with tropical total O_3 having undergone hardly any changes over the last decades (WMO, 2007).

References

Andersen, S. B., Weatherhead, E. C., Stevermer, A., Austin, J., Brühl, C., Fleming, E. L., Grandpré, J., Grewe, V., Isaksen, I., Pitari, G., Portmann, R. W., Rognerud, B., Rosenfield, J. E., Smyshlyaev, S., Nagashima, T., Velders, G. J. M., Weisenstein, D. K., and Xia, J.: Comparison of recent modeled and observed trends in total column ozone, J. Geophys. Res., 111, D02303, doi:10.1029/2005JD006091, 2006. 11271

Baldwin, M. P., Gray, L. J., Dunkerton, T. J., Hamilton, K., Haynes, P. H., Randel, W. J., Holton, J. R., Alexander, M. J., Hirota, I., Horinouchi, T., Jones, D. B. A., Kinnersley, J. S., Marquardt, C., Sata, K., and Takahashi, M.: The quasi-biennial oscillation, Rev. Geophys., 39, 179–229, doi:10.1029/1999RG000073, 2001. 11276

Bates, D. R. and Nicolet, M.: The photochemistry of atmospheric water vapour, J. Geophys. Res., 55, 301–327, doi:10.1029/JZ055i003p00301, 1950. 11271

Bauer, R., Rozanov, A., McLinden, C. A., Gordley, L. L., Lotz, W., Russell III, J. M., Walker, K. A., Zawodny, J. M., Ladstätter-Weißenmayer, A., Bovensmann, H., and Burrows, J. P.: Validation of SCIAMACHY limb NO_2 profiles using solar occultation measurements, Atmos. Meas. Tech., 5, 1059–1084, doi:10.5194/amt-5-1059-2012, 2012. 11272

Bernath, P. F., McElroy, C. T., Abrams, M. C., Boone, C. D., Butler, M., Camy-Peyret, C., Carleer, M., Clerbaux, C., Coheur, P.-F., Colin, R., DeCola, P., DeMazière, M., Drummond, J. R., Dufour, D., Evans, W. F. J., Fast, H., Fussen, D., Gilbert, K., Jennings, D. E., Llewellyn, E. J., Lowe, R. P., Mahieu, E., McConnell, J. C., McHugh, M., McLeod, S. D., Michaud, R., Midwinter, C., Nassar, R., Nichitiu, F., Nowlan, C., Rinsland, C. P., Rochon, Y. J., Rowlands, N., Semeniuk, K., Simon, P., Skelton, R., Sloan, J. J., Soucy, M.-A., Strong, K., Tremblay, P., Turnbull, D., Walker, K. A., Walkty, I., Wardle, D. A., Wehrle, V., Zander, R., and Zou, J.: Atmospheric Chemistry Experiment (ACE): mission overview, Geophys. Res. Lett., 32, L15S01, doi:10.1029/2005GL022386, 2005. 11272

Bovensmann, H., Burrows, J. P., Buchwitz, M., Frerick, J., Noël, S., Rozanov, V. V., Chance, K. V., and Goede, A. P. H.: SCIAMACHY: mission objectives and measurement modes, J. Atmos. Sci., 56, 127–150, 1999. 11274

Burrows, J. P., Hölzle, E., Goede, A. P. H., Visser, H., and Fricke, W.: SCIAMACHY – Scanning Imaging Absorption Spectrometer for Atmospheric Chartography, Acta Astronaut., 35, 445–451, 1995. 11274

Burrows, J. P., Weber, M., Buchwitz, M., Rozanov, V. V., Ladstätter-Weißenmayer, A., Richter, A., DeBeek, R., Hoogen, R., Bramstedt, K., and Eichmann, K.-U.: The Global Ozone Monitoring Experiment (GOME): mission concept and first scientific results, J. Atmos. Sci., 56, 151–174, 1999. 11273

Butchart, N., Scaife, A. A., Austin, J., Hare, S. H. E., and Knight, J. R.: Quasi-biennial oscillation in ozone in a coupled chemistry-climate model, J. Geophys. Res., 108, 4486, doi:10.1029/2002JD003004, 2003. 11276

Callies, J., Corpaccioli, E., Eisinger, M., Hahne, A., and Lefebvre, A.: GOME-2 – metop's second generation sensor for operational ozone monitoring, ESA Bull., 102, 28–36, 2000. 11273

Chen, W. and Huang, R.: The propagation and transport effect of planetary waves in the Northern Hemisphere winter, Adv. Atmos. Sci., 19, 1113–1126, 2002.

Chipperfield, M. P., Gray, L. J., Kinnersley, J. S., and Zawodny, J.: A two-dimensional model study of the QBO signal in SAGE II NO_2 and O_3, Geophys. Res. Lett., 21, 589–592, doi:10.1029/94GL00211, 1994. 11276

Stratospheric ozone trends and variability

C. Gebhardt et al.

Cochrane, D. and Orcutt, G. H.: Application of least squares regression to relationships containing autocorrelated error terms, J. Am. Stat. Assoc., 44, 32–61, 1949. 11274

Crutzen, P. J.: The influence of nitrogen oxides on the atmospheric ozone content, Q. J. Roy. Meteor. Soc., 96, 320–325, doi:10.1002/qj.49709640815, 1970. 11271

5   Dhomse, S., Weber, M., Wohltmann, I., Rex, M., and Burrows, J. P.: On the possible causes of recent increases in northern hemispheric total ozone from a statistical analysis of satellite data from 1979 to 2003, Atmos. Chem. Phys., 6, 1165–1180, doi:10.5194/acp-6-1165-2006, 2006. 11271, 11276

Ernst, F., von Savigny, C., Rozanov, A., Rozanov, V., Eichmann, K.-U., Brinkhoff, L. A.,
10   Bovensmann, H., and Burrows, J. P.: Global stratospheric aerosol extinction profile retrievals from SCIAMACHY limb-scatter observations, Atmos. Meas. Tech. Discuss., 5, 5993–6035, doi:10.5194/amtd-5-5993-2012, 2012. 11272

Farman, J. C., Gardiner, B. G., and Shanklin, J. D.: Large losses of total ozone in Antarctica reveal seasonal ClO_x/NO_x interaction, Nature, 315, 207–10, 1985. 11271

15   Fioletov, V. E.: Estimating the 27 day and 11 yr solar cycle variations in tropical upper stratospheric ozone, J. Geophys. Res., 114, D02302, doi:10.1029/2008JD010499, 2009. 11277

Fischer, H., Birk, M., Blom, C., Carli, B., Carlotti, M., von Clarmann, T., Delbouille, L., Dudhia, A., Ehhalt, D., Endemann, M., Flaud, J. M., Gessner, R., Kleinert, A., Koopman, R., Langen, J., López-Puertas, M., Mosner, P., Nett, H., Oelhaf, H., Perron, G., Remedios, J.,
20   Ridolfi, M., Stiller, G., and Zander, R.: MIPAS: an instrument for atmospheric and climate research, Atmos. Chem. Phys., 8, 2151–2188, doi:10.5194/acp-8-2151-2008, 2008. 11272

Fleming, E. L., Jackman, C. H., Stolarski, R. S., and Douglass, A. R.: A model study of the impact of source gas changes on the stratosphere for 1850–2100, Atmos. Chem. Phys., 11, 8515–8541, doi:10.5194/acp-11-8515-2011, 2011. 11281, 11288

25   Froidevaux, L., Jiang, Y. B., Lambert, A., Livesey, N. J., Read, W. G., Waters, J. W., Browell, E. V., Hair, J. W., Avery, M. A., McGee, T. J., Twigg, L. W., Sumnicht, G. K., Jucks, K. W., Margitan, J. J., Sen, B., Stachnik, R. A., Toon, G. C., Bernath, P. F., Boone, C. D., Walker, K. A., Filipak, M. J., Fuller, R. A., Manney, G. L., Schwartz, M. J., Daffer, W. H., Drouin, B. J., Cofield, R. E., Cuddy, D. T., Jarnot, R. F., Knosp, B. W., Perun, V. S.,
30   Snyder, W. V., Stek, P. K., Thurstans, R. P., and Wagner, P. A.: Validation of aura microwave limb sounder stratospheric ozone measurements, J. Geophys. Res., 113, D15S20, doi:10.1029/2007JD008771, 2008. 11284

Stratospheric ozone trends and variability

C. Gebhardt et al.

Title Page

Abstract | Introduction

Conclusions | References

Tables | Figures

|◄ | ►|

◄ | ►

Back | Close

Full Screen / Esc

Printer-friendly Version

Interactive Discussion

Gille, J., Barnett, J., Whitney, J., Dials, M., Woodard, D., Rudolf, W., Lambert, A., and Mankin, W.: The High Resolution Dynamics Limb Sounder (HIRDLS) experiment on aura, Proc. SPIE, 5152, 162–171, doi:10.1117/12.507657, 2003. 11272

Gray, L. J., Beer, J., Geller, M., Haigh, J. D., Lockwood, M., Matthes, K., Cubasch, U., Fleitmann, D., Harrison, G., Hood, L., Luterbacher, J., Meehl, G. A., Shindell, D., van Geel, B., and White, W.: Solar Influences on Climate, Rev. Geophys., 48, RG4001, doi:10.1029/2009RG000282, 2010. 11277

Harris, N. R. P., Kyrö, E., Staehelin, J., Brunner, D., Andersen, S.-B., Godin-Beekmann, S., Dhomse, S., Hadjinicolaou, P., Hansen, G., Isaksen, I., Jrrar, A., Karpetchko, A., Kivi, R., Knudsen, B., Krizan, P., Lastovicka, J., Maeder, J., Orsolini, Y., Pyle, J. A., Rex, M., Van-icek, K., Weber, M., Wohltmann, I., Zanis, P., and Zerefos, C.: Ozone trends at north-ern mid- and high latitudes – a European perspective, Ann. Geophys., 26, 1207–1220, doi:10.5194/angeo-26-1207-2008, 2008. 11271

Hasebe, F.: Quasi-biennial oscillations of ozone and diabatic circulation in the equatorial strato-sphere, J. Atmos. Sci., 51, 729–745, 1994.

Huang, F. T., Mayr, H. G., Russell III, J. M., and Mlynczak, M. G.: Ozone diurnal variations in the stratosphere and lower mesosphere, based on measurements from SABER on TIMED, J. Geophys. Res., 115, D24308, doi:10.1029/2010JD014484, 2010. 11283

Jarnot, R. F., Perun, V. S., and Schwartz, M. J.: Radiometric and spectral performance and calibration of the GHz bands of EOS MLS, IEEE T. Geosci. Remote Sens., 44, 1131–1143, doi:10.1109/TGRS.2005.863714, 2006. 11272, 11283

Jones, A., Urban, J., Murtagh, D. P., Eriksson, P., Brohede, S., Haley, C., Degenstein, D., Bourassa, A., von Savigny, C., Sonkaew, T., Rozanov, A., Bovensmann, H., and Burrows, J.: Evolution of stratospheric ozone and water vapour time series studied with satellite measure-ments, Atmos. Chem. Phys., 9, 6055–6075, doi:10.5194/acp-9-6055-2009, 2009. 11271, 11272, 11288

Kikuchi, K., Nishibori, T., Ochiai, S., Ozeki, H., Irimajiri, Y., Kasai, Y., Koike, M., Manabe, T., Mizukoshi, K., Murayama, Y., Nagahama, T., Sano, T., Sato, R., Seta, M., Takahashi, C., Takayanagi, M., Masuko, H., Inatani, J., Suzuki, M., and Shiotani, M.: Overview and early results of the Superconducting Submillimeter-Wave Limb-Emission Sounder (SMILES), J. Geophys. Res., 115, D23306, doi:10.1029/2010JD014379, 2010. 11273

Title Page

Abstract | Introduction

Conclusions | References

Tables | Figures

|◄ | ►|

◄ | ►

Back | Close

Full Screen / Esc

Printer-friendly Version

Interactive Discussion

Kühl, S., Pukite, J., Deutschmann, T., Platt, U., and Wagner, T.: SCIAMACHY limb measurements of NO_2, BrO, and OClO. Retrieval of vertical profiles: algorithm, first results, sensitivity and comparison studies, Adv. Space Res., 42, 1747–1764, 2008. 11272

Kyrölä, E., Tamminen, J., Leppelmeier, G. W., Sofieva, V., Hassinen, S., Bertaux, J. L., Hauchecorne, A., Dalaudier, F., Cot, C., Korablev, O., Fanton d'Andon, O., Barrot, G., Mangin, A., Théodore, B., Guirlet, M., Etanchaud, F., Snoeij, P., Koopman, R., Saavedra, L., Fraisse, R., Fussen, D., and Vanhellemont, F.: GOMOS on Envisat: an overview, Adv. Space Res., 33, 1020–1028, 2004. 11272

Lee, S., Shelow, D. M., Thompson, A. M., and Miller, S. K.: QBO and ENSO variability in temperature and ozone from SHADOZ (1998–2005), J. Geophys. Res., 115, D18105, doi:10.1029/2009JD013320, 2010. 11277

Llewellyn, E. J., Lloyd, N. D., Degenstein, D. A., Gattinger, R. L., Petelina, S. V., Bourassa, A. E., Wiensz, J. T., Ivanov, E. V., McDade, I. C., Solheim, B. H., McConnell, J. C., Haley, C. S., von Savigny, C., Sioris, C. E., McLinden, C. A., Griffioen, E., Kaminski, J., Evans, W. F. J., Puckrin, E., Strong, K., Wehrle, V., Hum, R. H., Kendall, D. J. W., Matsushita, J., Murtagh, D. P., Brohede, S., Stegman, J., Witt, G., Barnes, G., Payne, W. F., Piché, L., Smith, K., Warshaw, G., Deslauniers, D.-L., Marchand, P., Richardson, E. H., King, R. A., Wevers, I., McCreath, W., Kyrölä, E., Oikarinen, L., Leppelmeier, G. W., Auvinen, H., Mégie, G., Hauchecorne, A., Lefèvre, F., de La Nöe, J., Ricaud, P., Frisk, U., Sjoberg, F., von Schéele, F., and Nordh, L.: The OSIRIS instrument on the Odin spacecraft, Can. J. Phys., 82, 411–422, 2004. 11273, 11282

Lucke, R. L., Korwan, D. R., Bevilacqua, R. M., Hornstein, J. S., Shettle, E. P., Chen, D. T., Daehler, M., Lumpe, J. D., Fromm, M. D., Debrestian, D., Neff, B., Squire, M., König-Langlo, G., and Davies, J.: The Polar Ozone and Aerosol Measurement (POAM) III instrument and early validation results, J. Geophys. Res., 104, 18785–18799, doi:10.1029/1999JD900235, 1999. 11273

Mauldin III, L. E., Zaun, N., McCormick, M. P., Guy, J. H., and Vaugh, W. R.: Stratospheric Aerosol and Gas Experiment II instruments: a functional description, Opt. Eng., 24, 307–312, 1985. 11273

McElroy, M. B., Salawitch, R. J., Wofsy, S. C., and Logan, J. A.: Reductions of Antarctic ozone due to synergistic interactions of chlorine and bromine, Nature, 321, 759–762, 1986. 11271

Mieruch, S., Weber, M., von Savigny, C., Rozanov, A., Bovensmann, H., Burrows, J. P., Bernath, P. F., Boone, C. D., Froidevaux, L., Gordley, L. L., Mlynczak, M. G., Russell III, J. M.,

Thomason, L. W., Walker, K. A., and Zawodny, J. M.: Global and long-term comparison of SCIAMACHY limb ozone profiles with correlative satellite data (2002–2008), Atmos. Meas. Tech., 5, 771–788, doi:10.5194/amt-5-771-2012, 2012. 11271, 11272, 11281, 11287

Miller, A. J., Airong, C., George, T., Wuebbles, D. J., Flynn, L. E., Shi-Keng, Y., Weatherhead, E. C., Fioletov, V., Petropavlovskikh, I., Meng, X.-L., Guillas, S., Nagatani, R. M., and Reinsel, G. C.: Examination of ozonesonde data for trends and trend changes incorporating solar and Arctic oscillation signals, J. Geophys. Res., 111, D13305, doi:10.1029/2005JD006684, 2006. 11271

Molina, M. J. and Rowland, F. S.: Stratospheric sink for chlorofluoromethanes: chlorine atom-catalysed destruction of ozone, Nature, 249, 810–812, 1974. 11271

Murtagh, D., Frisk, U., Merino, F., Ridal, M., Jonsson, A., Stegman, J., Witt, G., Eriksson, P., Jiménez, C., Mégie, G., de la No, J., Ricaud, P., Baron, P., Pardo, J. R., Hauchcorne, A., Llewellyn, E. J., Degenstein, D. A., Gattinger, R. L., Lloyd, N. D., Evans, W. F. J., McDade, I. C., Haley, C. S., Sioris, C., v. Savigny, C., Solheim, B. H., McConnell, J. C., Strong, K., Richardson, E. H., Leppelmeier, G. W., Kyrölä, E., Auvinen, H, and Oikarinen, L.: An overview of the Odin atmospheric mission, Can. J. Phys., 80, 309–319, doi:10.1139/p01-157, 2002. 11273

Naujokat, B.: An update of the observed Quasi-Biennial Oscillation of stratospheric winds over the tropics, J. Atmos. Sci., 43, 1873–1877, 1986. 11276

Nevison, C. D., Solomon, S., and Gao, R. S.: Buffering interactions in the modeled response of stratospheric O_3 to increased NO_x and HO_x, J. Geophys. Res., 104, 3741–3754, doi:10.1029/1998JD100018, 1999. 11280, 11288

Newchurch, M. J., Yang, E.-S., Cunnold, D. M., Reinsel, G. C., Zawodny, J. M., and Russell III, J. M.: Evidence for slowdown in stratospheric ozone loss: first stage of ozone recovery, J. Geophys. Res., 108, 4507, doi:10.1029/2003JD003471, 2003. 11271, 11282

Osterman, G. B., Salawitch, R. J., Sen, B., Toon, G. C., Stachnik, R. A., Pickett, H. M., Margitan, J. J., Blavier, J.-F., and Peterson, D. B.: Balloon-borne measurements of stratospheric radicals and their precursors: implications for the production and loss of ozone, Geophys. Res. Lett., 24, 1107–1110, doi:10.1029/97GL00921, 1997. 11271

Perliski, L. M., Solomon, S., and London, J.: On the interpretation of seasonal variations of stratospheric ozone, Planet. Space Sci., 37, 1527–1538, 1989. 11278, 11279

Portmann, R. W. and Solomon, S.: Indirect radiative forcing of the ozone layer during the 21st century, Geophys. Res. Lett., 34, L02813, doi:10.1029/2006GL028252, 2007. 11281, 11288

Title Page

Abstract | Introduction

Conclusions | References

Tables | Figures

◄◄ | ►►

◄ | ►

Back | Close

Full Screen / Esc

Printer-friendly Version

Interactive Discussion

Randel, W. J. and Thompson, A. M.: Interannual variability and trends in tropical ozone derived from SAGE II satellite data and SHADOZ ozonesondes, J. Geophys. Res., 116, D07303, doi:10.1029/2010JD015195, 2011. 11271, 11272, 11277, 11280, 11286, 11287

Randel, W. J. and Wu, F.: A stratospheric ozone profile data set for 1979–2005: variability, trends, and comparisons with column ozone data, J. Geophys. Res., 112, D06313, doi:10.1029/2006JD007339, 2007. 11271

Randel, W. J., Garcia, R. R., Calvo, N., and Marsh, D.: ENSO influence on zonal mean temperature and ozone in the tropical lower stratosphere, Geophys. Res. Lett., 36, L15822, doi:10.1029/2009GL039343, 2009. 11277

Reinsel, G. C.: Trend analysis of upper stratospheric Umkehr ozone data for evidence of turnaround, Geophys. Res. Lett., 29, 1451, doi:10.1029/2002GL014716, 2002. 11271, 11282

Reinsel, G. C., Miller, A. J., Weatherhead, E. C., Flynn, L. E., Nagatani, R. M., Tiao, G. C., and Wuebbles, D. J.: Trend analysis of total ozone data for turnaround and dynamical contributions, J. Geophys. Res., 110, D16306, doi:10.1029/2004JD004662, 2005. 11271

Remsberg, E. and Lingenfelser, G.: Analysis of SAGE II ozone of the middle and upper stratosphere for its response to a decadal-scale forcing, Atmos. Chem. Phys., 10, 11779–11790, doi:10.5194/acp-10-11779-2010, 2010. 11277

Rosenfield, J. E., Frith, S. M., and Stolarski, R. S.: Version 8 SBUV ozone profile trends compared with trends from a zonally averaged chemical model, J. Geophys. Res., 110, D12302, doi:10.1029/2004JD005466, 2005. 11271

Rozanov, A., Eichmann, K.-U., von Savigny, C., Bovensmann, H., Burrows, J. P., von Bargen, A., Doicu, A., Hilgers, S., Godin-Beekmann, S., Leblanc, T., and McDermid, I. S.: Comparison of the inversion algorithms applied to the ozone vertical profile retrieval from SCIAMACHY limb measurements, Atmos. Chem. Phys., 7, 4763–4779, doi:10.5194/acp-7-4763-2007, 2007. 11272

Rozanov, A., Kühl, S., Doicu, A., McLinden, C., Pukite, J., Bovensmann, H., Burrows, J. P., Deutschmann, T., Dorf, M., Goutail, F., Grunow, K., Hendrick, F., von Hobe, M., Hrechanyy, S., Lichtenberg, G., Pfeilsticker, K., Pommereau, J. P., Van Roozendael, M., Stroh, F., and Wagner, T.: BrO vertical distributions from SCIAMACHY limb measurements: comparison of algorithms and retrieval results, Atmos. Meas. Tech., 4, 1319–1359, doi:10.5194/amt-4-1319-2011, 2011. 11272

Title Page

Abstract | Introduction

Conclusions | References

Tables | Figures

◄◄ | ►►

◄ | ►

Back | Close

Full Screen / Esc

Printer-friendly Version

Interactive Discussion

Russell III, J. M., Gordley, L. L., Park, J. H., Drayson, S. R., Hesketh, W. D., Cicerone, R. J., Tuck, A. F., Frederick, J. E., Harries, J. E., and Crutzen, P. J.: The Halogen Occultation Experiment, J. Geophys. Res., 98, 777–797, doi:10.1029/93JD00799, 1993. 11272

Salawitch, R. J., Weisenstein, D. K., Kovalenko, L. J., Sioris, C. E., Wennberg, P. O., Chance, K., Ko, M. K. W., and McLinden, C. A.: Sensitivity of ozone to bromine in the lower stratosphere, Geophys. Res. Lett., 32, L05811, doi:10.1029/2004GL021504, 2005.

Schmidt, H., Brasseur, G. P., and Giorgetta, M. A.: Solar cycle signal in a general circulation and chemistry model with internally generated quasi-biennial oscillation, J. Geophys. Res., 115, D00I14, doi:10.1029/2009JD012542, 2010.

Sioris, C. E., Haley, C. S., McLinden, C. A., v. Savigny, C., McDade, I. C., McConnell, J. C., Evans, W. F. J., Lloyd, N. D., Llewellyn, E. J., Chance, K. V., Kurosu, T. P., Murtagh, D., Frisk, U., Pfeilsticker, K., Bösch, H., Weidner, F., Strong, K., Stegman, J., and Mégie, G.: Stratospheric profiles of nitrogen dioxide observed by Optical Spectrograph and Infrared Imager System on the Odin satellite, J. Geophys. Res., 108, 4215, doi:10.1029/2002JD002672, 2003. 11272

Sioris, C. E., Kurosu, T. P., Martin, R. V., and Chance, K.: Stratospheric and tropospheric NO_2 observed by SCIAMACHY: first results, Adv. Space Res., 34, 780–785, doi:10.1016/j.asr.2003.08.066, 2004. 11272

Soukharev, B. E. and Hood, L. L.: Solar cycle variation of stratospheric ozone: multiple regression analysis of long-term satellite data sets and comparisons with models, J. Geophys. Res., 111, D20314, doi:10.1029/2006JD007107, 2006. 11277

SPARC CCMVal: SPARC Report on the Evaluation of Chemistry-Climate Models, edited by: Eyring, V., Shepherd, T. G., and Waugh D. W., SPARC Report No. 5, WCRP-132, WMO/TD-No. 1526, http://www.atmosp.physics.utoronto.ca/SPARC, 2010. 11277

Steinbrecht, W., Claude, H., Schönenborn, F., McDermid, I. S., Leblanc, T., Godin, S., Song, T., Swart, D. P. J., Meijer, Y. J., Bodeker, G. E., Connor, B. J., Kämpfer, N., Hocke, K., Calisesi, Y., Schneider, N., de la Noë, J., Parrish, A. D., Boyd, I. S., Brühl, C., Steil, B., Giorgetta, M. A., Manzini, E., Thomason, L. W., Zawodny, J. M., McCormick, M. P., Russel III, J. M., Bhartia, P. K., Stolarski, R. S., and Hollandsworth-Frith, S. M.: Long-term evolution of upper stratospheric ozone at selected stations of the Network for the Detection of Stratospheric Change (NDSC), J. Geophys. Res., 111, D10308, doi:10.1029/2005JD006454, 2006. 11271, 11272, 11282, 11288

Steinbrecht, W., Claude, H., Schönenborn, F., McDermid, I. S., Leblanc, T., Godin-Beekmann, S., Keckhut, P., Hauchecorne, A., Van Gijsel, J. A. E., Swart, D. P. J., Bodeker, G. E., Parrish, A., Boyd, I. S., Kämpfer, N., Hocke, K., Stolarski, R. S., Frith. S. M., Thomason, L. W., Remsberg, E. E., v. Savigny, C., Rozanov, A., and Burrows, J. P.: Ozone and temperature trends in the upper stratosphere at five stations of the Network for the Detection of Atmospheric Composition Change, Int. J. Remote Sens., 30, 3875–2886, 2009. 11272, 11282, 11288

Stiller, G. P., von Clarmann, T., Haenel, F., Funke, B., Glatthor, N., Grabowski, U., Kellmann, S., Kiefer, M., Linden, A., Lossow, S., and López-Puertas, M.: Observed temporal evolution of global mean age of stratospheric air for the 2002 to 2010 period, Atmos. Chem. Phys., 12, 3311–3331, doi:10.5194/acp-12-3311-2012, 2012. 11275, 11282

Stolarski, R. S. and Cicerone, R. J.: Stratospheric chlorine: a possible sink for ozone, Can. J. Chem., 52, 1610–1615, doi:10.1139/v74-233, 1974. 11271

Thompson, A. M., Witte, J. C., McPeters, R. D., Oltmans, S. J., Schmidlin, F. J., Logan, J. A., Fujiwara, M., Kirchhoff, V. W. J. H., Posny, F., Coetzee, G. J. R., Hoegger, B., Kawakami, S., Ogawa, T., Johnson, B. J., Vömel, H., and Labow, G.: Southern Hemisphere Additional Ozonesondes (SHADOZ) 1998–2000 tropical ozone climatology 1. Comparison with Total Ozone Mapping Spectrometer (TOMS) and ground-based measurements, J. Geophys. Res., 108, 8238, doi:10.1029/2001JD000967, 2003. 11286

Thompson, A. M., Allen, A. L., Lee, S., Miller, S. K., and Witte, J. C.: Gravity and Rossby wave signatures in the tropical troposphere and lower stratosphere based on Southern Hemisphere Additional Ozonesondes (SHADOZ), 1998–2007, J. Geophys. Res., 116, D05302, doi:10.1029/2009JD013429, 2011. 11277

Tiao, G. C., Reinsel, G. C., Xu, D., Pedrick, J. H., Zhu, X., Miller, A. J., DeLuisi, J. J., Mateer, C. L., and Wuebbles, D. J.: Effects of autocorrelation and temporal sampling schemes on estimates of trend and spatial correlation, J. Geophys. Res., 95, 20507–20517, doi:10.1029/JD095iD12p20507, 1990. 11275

Viereck, R., Puga, L., McMullin, D., Judge, D., Weber, M., and Tobiska, W. K.: The Mg II index: a proxy for solar EUV, Geophys. Res. Lett., 28, 1343–1346, doi:10.1029/2000GL012551, 2001. 11277

Viereck, R. A., Floyd, L. E., Crane, P. C., Woods, T. N., Knapp, B. G., Rottman, G., Weber, M., Puga, L. C., and DeLand, M. T.: A composite Mg II index spanning from 1978 to 2003, Adv. Space Res., 2, S10005, doi:10.1029/2004SW000084, 2004. 11277

Title Page

Abstract | Introduction

Conclusions | References

Tables | Figures

|◄ | ►|

◄ | ►

Back | Close

Full Screen / Esc

Printer-friendly Version

Interactive Discussion

Weber, M., Dikty, S., Burrows, J. P., Garny, H., Dameris, M., Kubin, A., Abalichin, J., and Langematz, U.: The Brewer–Dobson circulation and total ozone from seasonal to decadal time scales, Atmos. Chem. Phys., 11, 11221–11235, doi:10.5194/acp-11-11221-2011, 2011. 11270

Weber, M., Steinbrecht, W., Long, C. S., Fioletov, V. E., Frith, S. H., Stolarski, R. S., and Newman, P. A.: [Global climate] stratospheric ozone [in state of the climate in 2011], B. Am. Meteorol. Soc., 93, S46–S48, 2012. 11287

Weber, M., Pagaran, J., Dikty, S., von Savigny, C., Burrows, J. P, DeLand, M., Floyd, L. E., Harder, J. W., Mlynczak, M. G., and Schmidt, H.: Investigation of solar irradiance variations and their impact on middle atmospheric ozone, Chapter 3, doi:10.1007/978-94-007-4348-9_3, in: Climate And Weather of the Sun-Earth System (CAWSES): Highlights from a Priority Program, edited by: Lübken, F.-J., Springer, Dordrecht, the Netherlands, 2013. 11277

World Meteorological Organization: Scientific Assessment of Ozone Depletion, 1998, WMO Global Ozone Research and Monitoring Project – Report No. 44, 1999. 11272, 11282, 11288

World Meteorological Organization: Scientific Assessment of Ozone Depletion, 2006, WMO Global Ozone Research and Monitoring Project – Report No. 50, 2007. 11271, 11289

World Meteorological Organization: Scientific Assessment of Ozone Depletion, 2010, WMO Global Ozone Research and Monitoring Project – Report No. 52, 2011. 11271, 11288

Yang, E.-S., Cunnold, D. M., Salawitch, R. J., McCormick, M. P., Russell III, J. M., Zawodny, J. M., Oltmans, S., and Newchurch, M. J.: Attribution of recovery in lower-stratospheric ozone, J. Geophys. Res., 111, D17309, doi:10.1029/2005JD006371, 2006. 11271, 11280

Zanis, P., Maillard, E., Staehelin, J., Zerefos, C., Kosmidis, E., Tourpali, K., Wohltmann, I.: On the turnaround of stratospheric ozone trends deduced from the reevaluated Umkehr record of Arosa, Switzerland, J. Geophys. Res., 111, D22, doi:10.1029/2005JD006886, 2006. 11271

Zawodny, J. M. and McCormick, M. P.:, Stratospheric Aerosol and Gas Experiment II measurements of the quasi-biennial oscillations in ozone and nitrogen dioxide, J. Geophys. Res., 96, 9371–9377, doi:10.1029/91JD00517, 1991. 11276

Ziemke, J. R., Chandra, S., Oman, L. D., and Bhartia, P. K.: A new ENSO index derived from satellite measurements of column ozone, Atmos. Chem. Phys., 10, 3711–3721, doi:10.5194/acp-10-3711-2010, 2010. 11277

Title Page

Abstract | Introduction

Conclusions | References

Tables | Figures

|◄ | ►|

◄ | ►

Back | Close

Full Screen / Esc

Printer-friendly Version

Interactive Discussion
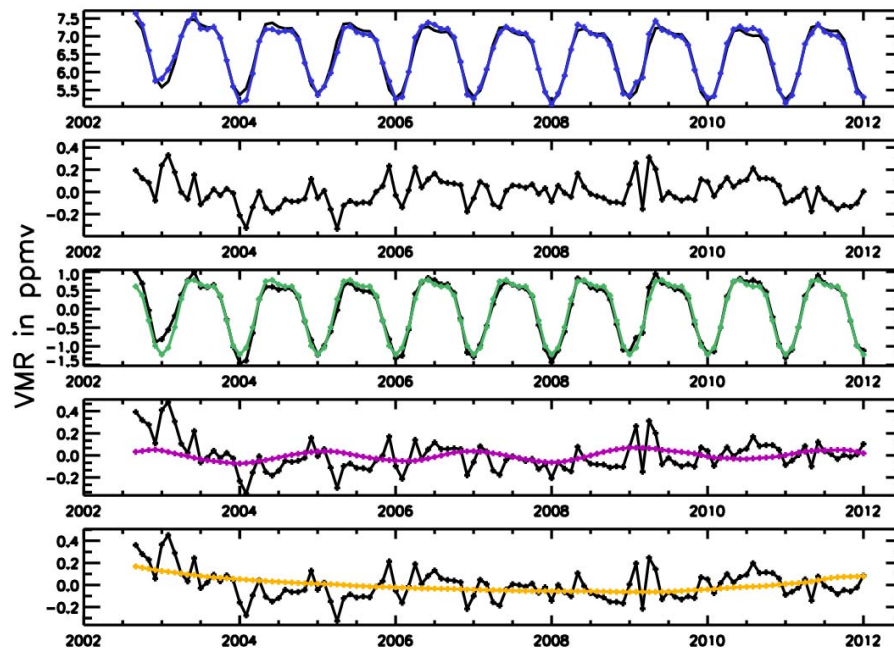
Fig. 1. SCIAMACHY O_3 time series at 35 km for 60–50° N (blue) with overlaid fitting curve (black) in top panel and fit residuals (second panel). Below (from top to bottom): harmonic terms (green) overlaid by detrended time series, QBO terms (magenta) overlaid by detrended and deseasonalised time series, and solar cycle terms (orange) overlaid by time series with all other terms removed.

Printer-friendly Version

Interactive Discussion
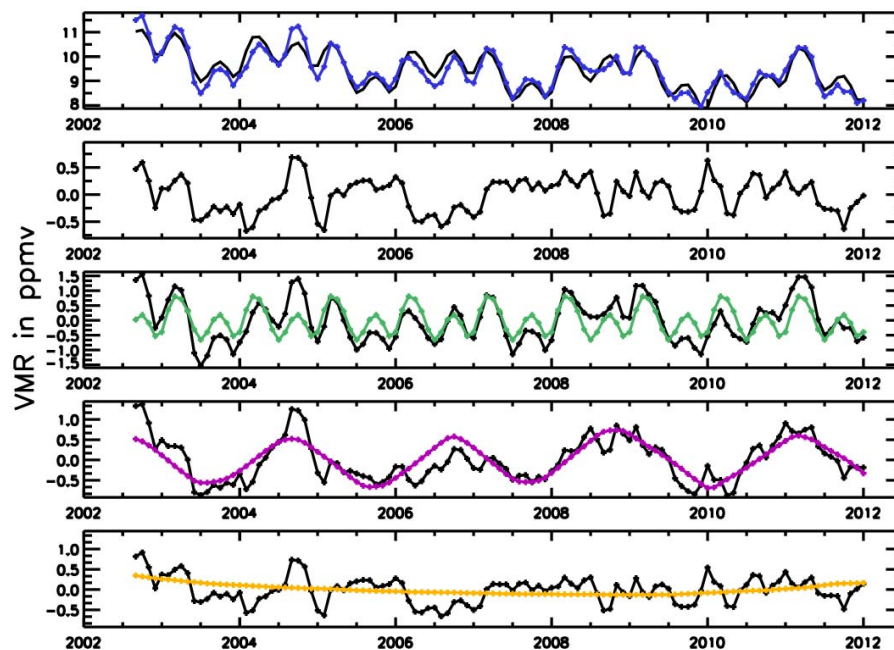
Fig. 2. Same as Fig. 1 but for 5° N–5° S.
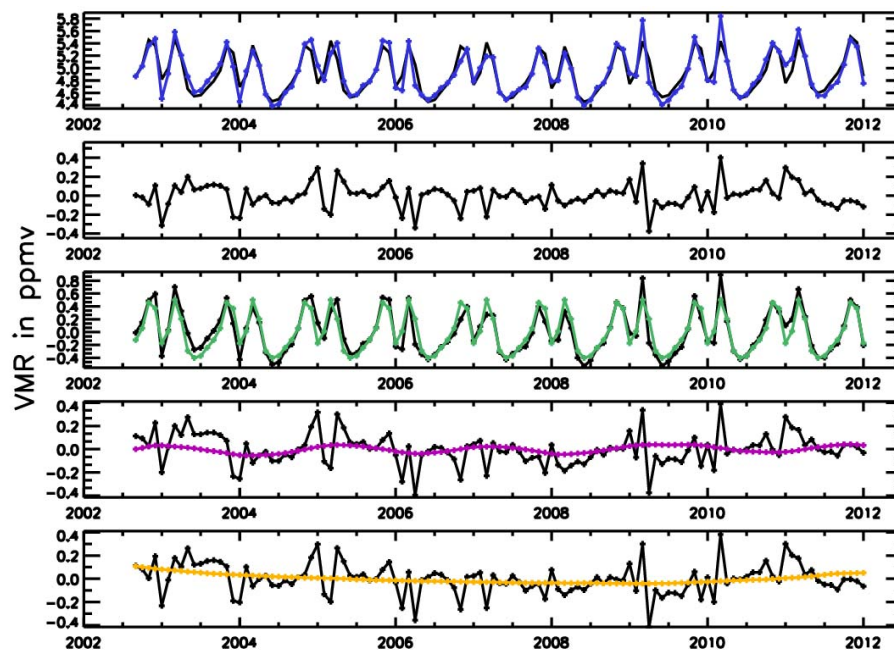
Fig. 3. Same as Fig. 1 but at 44 km altitude.
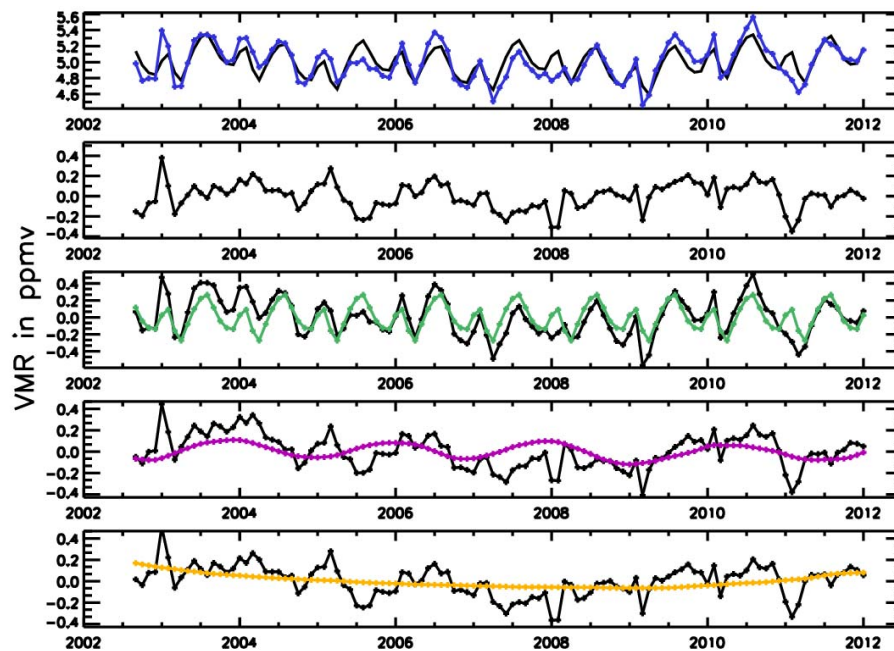
Fig. 4. Same as Fig. 3 but for 5° N–5° S.
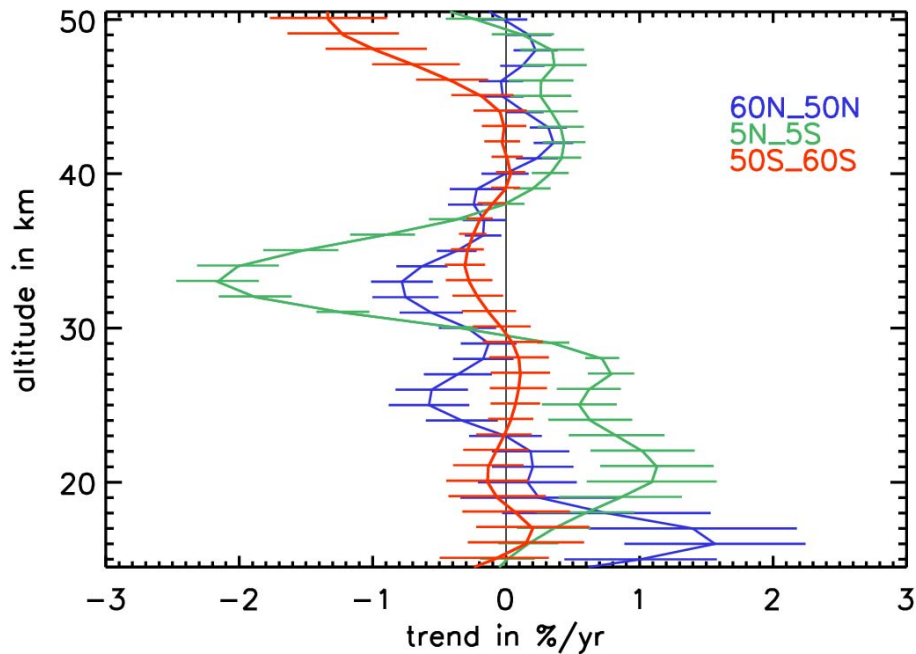
Fig. 5. Ozone trend profiles inferred from SCIAMACHY limb measurements for the latitude bands 60–50° N, 5° N–5° S, and 50–60° S. Error bars: 1σ.
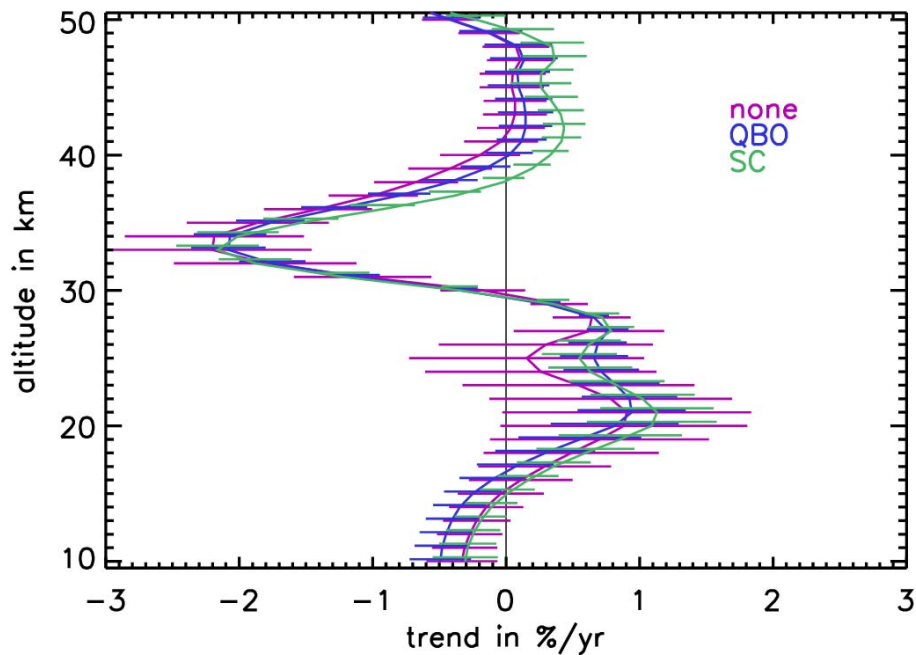
Fig. 6. SCIAMACHY ozone trends for the 5° N–5° S latitude band determined without QBO and solar cycle (magenta), with QBO but without solar cycle (blue), and with both accounted for (green). Error bars: 1σ.
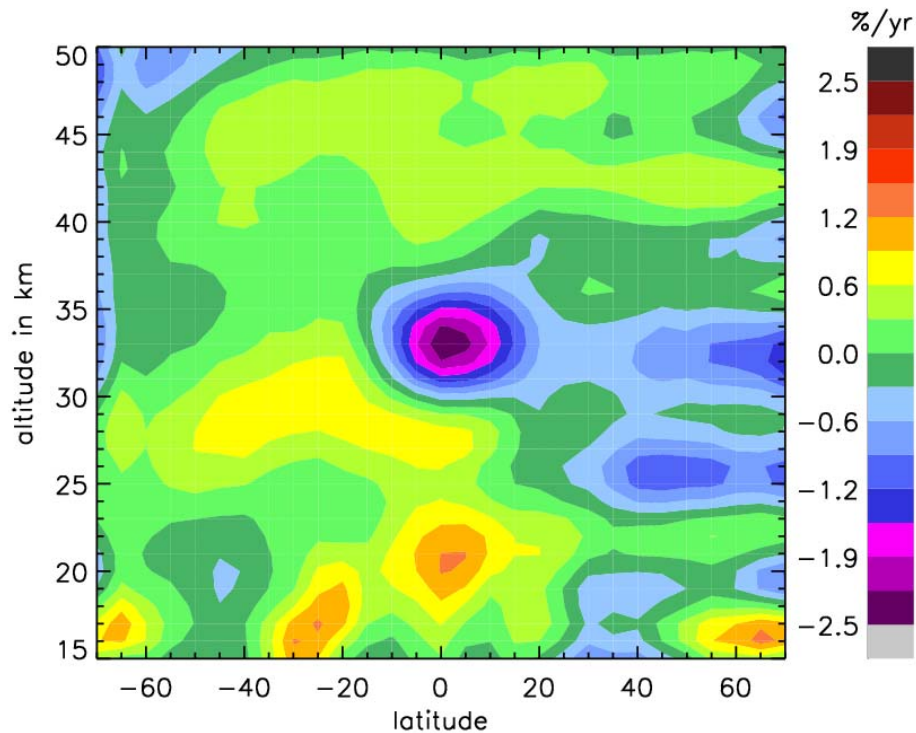
Fig. 7. Latitude-altitude cross section of ozone trends from SCIAMACHY: latitude range from 70° N–70° S, altitude range from 15–50 km. Legend on the right: units of % yr^{-1}.

Title Page

Abstract | Introduction

Conclusions | References

Tables | Figures

|◄ | ►|

◄ | ►

Back | Close

Full Screen / Esc

Printer-friendly Version

Interactive Discussion

Fig. 8. Ozone trends inferred from SCIAMACHY and MLS measurements: 60–50° N, August 2004–December 2011. Error bars: 1σ.
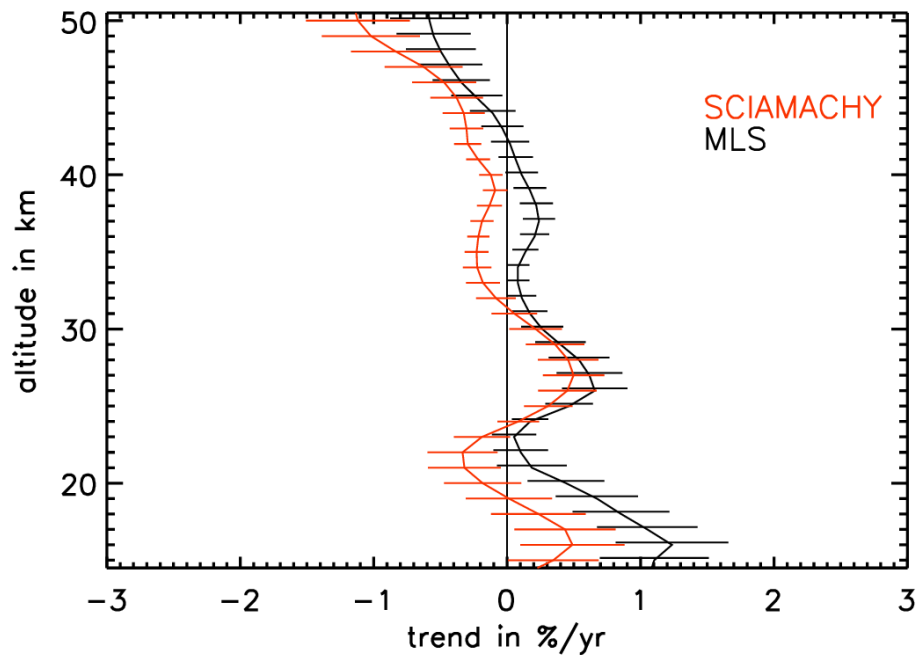
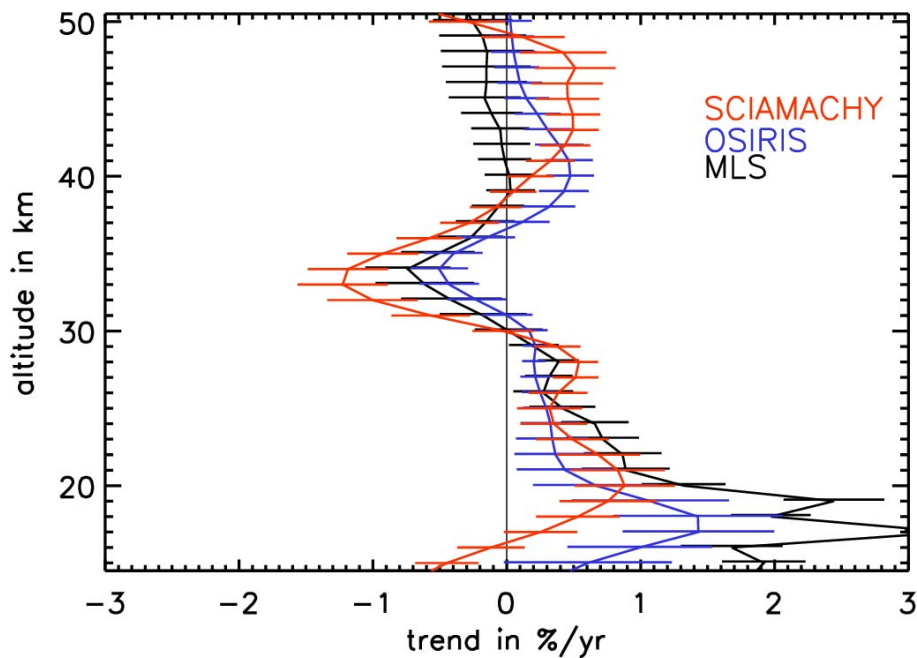**Fig. 9.** Ozone trends inferred from SCIAMACHY and MLS measurements: 50–60° S, August 2004–December 2011. Error bars: 1σ.

Title Page

Abstract | Introduction

Conclusions | References

Tables | Figures

◄ | ►

◄ | ►

Back | Close

Full Screen / Esc

Printer-friendly Version

Interactive Discussion
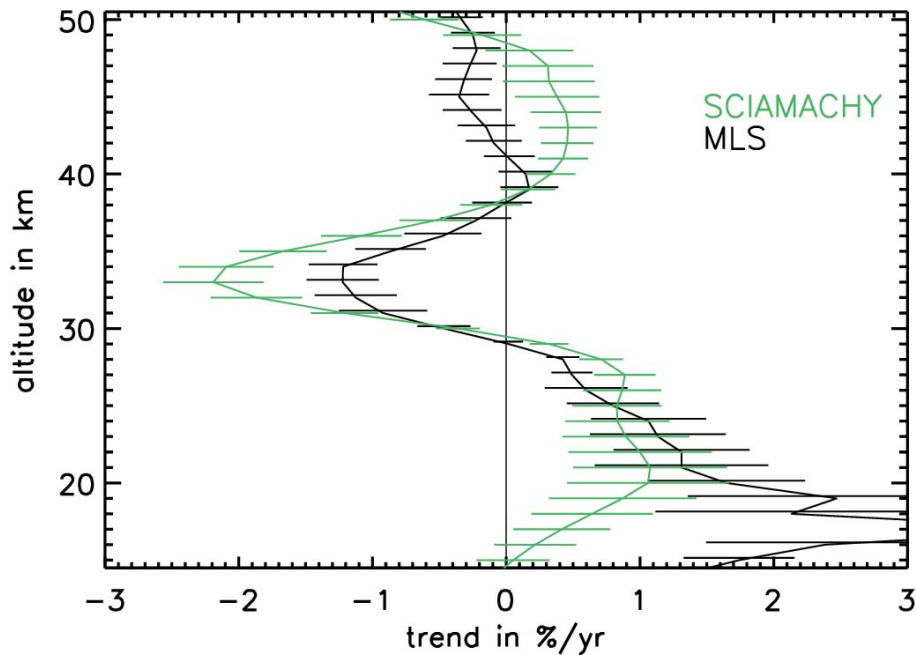
Fig. 10. Ozone trends inferred from SCIAMACHY and MLS measurements: 5° N–5° S, August 2004–December 2011. Error bars: 1σ.
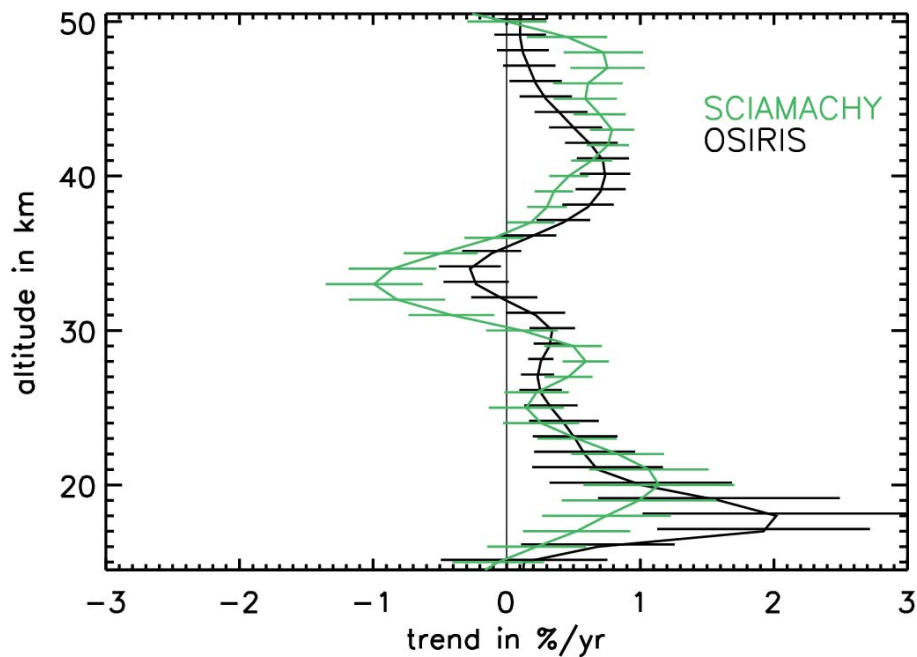
Fig. 11. Ozone trends inferred from SCIAMACHY and OSIRIS measurements: 20° N–20° S, August 2002–December 2011. Error bars: 1σ.

Fig. 12. Ozone trends inferred from SCIAMACHY, MLS, and OSIRIS measurements: 20° N–20° S, August 2004–December 2011. Error bars: 1σ.

Title Page

Abstract | Introduction

Conclusions | References

Tables | Figures

|◄ | ►|

◄ | ►

Back | Close

Full Screen / Esc

Printer-friendly Version

Interactive Discussion
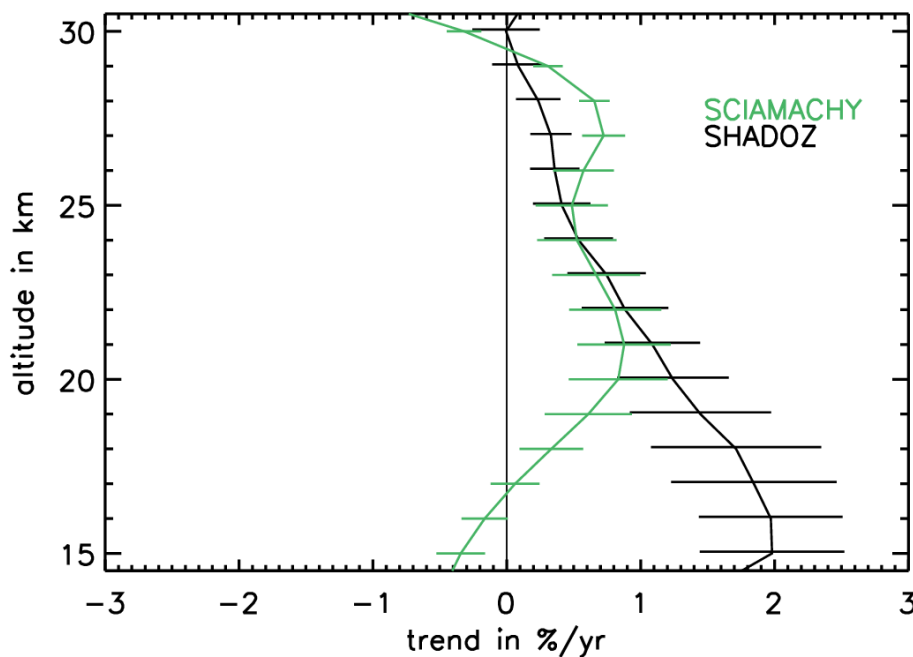
Fig. 13. Ozone trends inferred from SCIAMACHY and from average of tropical SHADOZ ozonesonde stations including Ascension (8.0° S, 14.4° W), Kuala Lumpur (2.7° N, 101.7° E), Nairobi (1.3° S, 36.8° E), Natal (5.4° S, 35.4° W), and Paramaribo (5.8° N, 55.2° W). Error bars: 1σ.

Title Page

Abstract | Introduction

Conclusions | References

Tables | Figures

◀ | ▶|

◀ | ▶

Back | Close

Full Screen / Esc
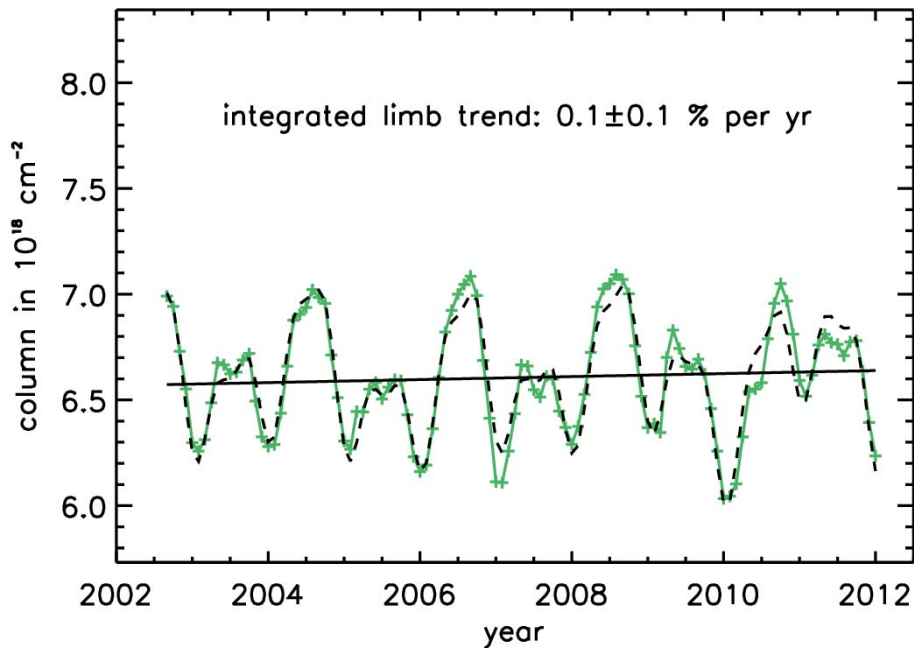
Printer-friendly Version

Interactive Discussion

Fig. 14. Limb ozone from SCIAMACHY for 5° N–5° S integrated from 10–75 km (green). The overall fitting curve (black dashed) and its linear terms (black) are overlaid.

Title Page

Abstract | Introduction

Conclusions | References

Tables | Figures

|◄ | ►|

◄ | ►

Back | Close

Full Screen / Esc

Printer-friendly Version
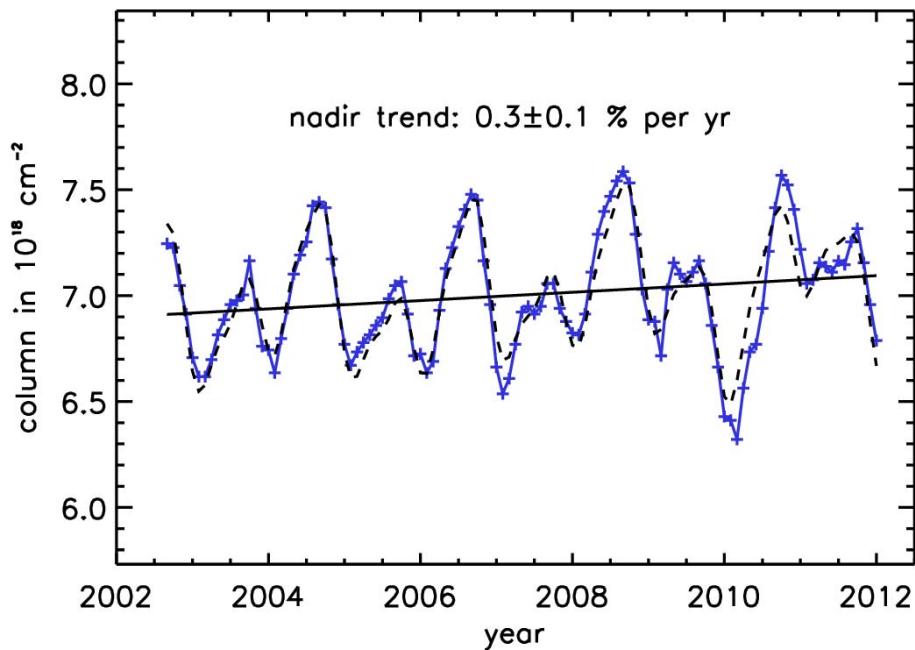
Interactive Discussion

Fig. 15. Nadir total ozone for 5° N–5° S from a merged dataset from GOME, SCIAMACHY nadir, and GOME2 (blue). The overall fitting curve (black dashed) and its linear terms (black) are overlaid.

Title Page

Abstract | Introduction

Conclusions | References

Tables | Figures

|◀ | ▶|

◀ | ▶

Back | Close

Full Screen / Esc

Printer-friendly Version

Interactive Discussion